Available online at www.sciencedirect.com
ScienceDirect
Journal of Nuclear Materials 363–365 (2007) 359–364
journal of nuclear materials
www.elsevier.com/locate/jnucmat

Measurement and modeling of detached plasma cooling via ro-vibrational excitation of H_2 neutrals in PISCES-A

E.M. Hollmann *, A.Yu. Pigarov [1], Z. Yan

University of California, San Diego, 9500 Gilman Drive La Jolla, CA 92093-0417, USA

Abstract

Measurements of the spatial decay of H_2 vibrational, rotational, and kinetic temperatures T_{vib}, T_{rot}, and T_{kin} down the side port of the PISCES-A vacuum chamber, together with Monte-Carlo modeling, is used to obtain the accommodation probabilities for energy loss to the cold chamber walls during H_2 + surface collisions. These accommodation probabilities are used to calculate the steady-state rate at which H_2 carries energy away from the plasma column. The power loss due to heating of H_2 neutrals is found to be quite significant, being only $2\times$ weaker than radiation cooling in the higher neutral pressure (detached) discharges. The H_2 vibrational temperature T_{vib} is found to be the most important neutral channel for carrying energy out of the plasma – more important than either kinetic temperature T_{kin} or rotational temperature T_{rot}.
© 2007 Elsevier B.V. All rights reserved.

PACS: 34.50.Ez; 52.20.Hv; 52.25.Ya

Keywords: Hydrogen molecules; Rotational and vibrational excitation; Neutral gas modeling; Heat load reduction

1. Introduction

In magnetic fusion experiments, hydrogen molecules (e.g. H_2, D_2, and/or T_2) are the dominant neutral species recycled from the wall under normal operating conditions [1] and play an important role in the chemical processes occurring in the plasma edge, in particular in the detached divertor region [2]. For example, the formation and subsequent recombination of molecular or negative hydrogenic ions, e.g. H_2^+ and H^- require the presence of hydrogen molecules [3]. Additionally, hydrogen molecules could play an important role in cooling the plasma edge. Although the role of hydrogen atoms (e.g. H or D) in cooling edge plasmas has been studied extensively, e.g. [4], very little work has been done on the degree of plasma cooling resulting from the presence of hydrogen molecules in the edge region.

Here, a linear divertor simulator experiment is used to study the magnitude of the plasma cooling occurring due to the presence of hydrogen molecules in weakly-ionized hydrogen discharges. This is accomplished by measuring the H_2 vibrational, rotational, and kinetic temperatures T_{vib}, T_{rot}, and T_{kin} both in the plasma and near the end of a side port using visible spectroscopy. Monte-Carlo modeling of the H_2 trajectories is then used to

* Corresponding author.
E-mail addresses: ehollmann@ucsd.edu (E.M. Hollmann), apigarov@ucsd.edu (A.Yu. Pigarov).
[1] Presenting author.

0022-3115/$ - see front matter © 2007 Elsevier B.V. All rights reserved.
doi:10.1016/j.jnucmat.2007.01.031

obtain the accommodation probabilities, i.e. the cooling probability for T_{vib}, T_{rot}, and T_{kin} to the wall temperature in H_2-surface collisions. The accommodation probabilities are then used to calculate the steady-state plasma cooling rate due to ro-vibrational and kinetic heating of H_2 molecules. For high neutral pressures ($P > 10$ mTorr), neutral cooling is found to be a significant energy loss channel, being only a factor two smaller than radiation. The H_2 vibrational temperature T_{vib} is found to be the most important channel for carrying neutral energy out of the plasma – more important than either kinetic temperature T_{kin} or rotational temperature T_{rot}. These results demonstrate the importance of including of H_2 neutrals in understanding power balance in detached tokamak divertors.

2. Experimental set up

The experiments discussed here were performed in the PISCES-A linear divertor simulator experiment [5]. An overview of the experimental setup used is shown in Fig. 1. A steady-state reflex-arc plasma discharge is used. Typical discharge powers are $80\ \mathrm{V} \times 30\ \mathrm{A} = 2.4\ \mathrm{kW}$. The target region pressure $P = 1$–20 mTorr is varied experimentally by changing the fueling rate and pumping rates of H_2 gas into/out of the target chamber. The experiments discussed here are all performed in the target region, which has dimensions length $L_w = 70$ cm and radius $R_w = 9.8$ cm.

Plasma electron density n_e and electron temperature T_e are measured using a plunging probe. Neutral pressure in the target region was measured using a baratron gauge. Plasma visible line emission is measured using a 1.3 m Czerny–Turner visible spectrometer. This spectrometer was equipped with views of either the plasma or a weak electron beam installed in a side port (as shown in Fig. 1(b)), allowing measurement of the H_2 temperatures either in the plasma or in the side port. The electronic ground state H_2 temperatures T_{vib} and T_{rot} are obtained using measurements of the Fulcher band [(1s)3p-(1s)2s triplet Q-branch, $d^3\Pi_u^- \rightarrow a^3\Sigma_g^+$] of H_2. This technique has been discussed in detail previously [6,7]. The H_2 translational temperature T_{kin} is obtained from the line width of a strong Fulcher band line [usually $Q1(V = 0)$] deconvolved with the instrumental broadening.

Radial profiles of electron density and temperature (n_e, T_e) measured with the Langmuir probe and line-integrated profiles of the H_2 temperatures

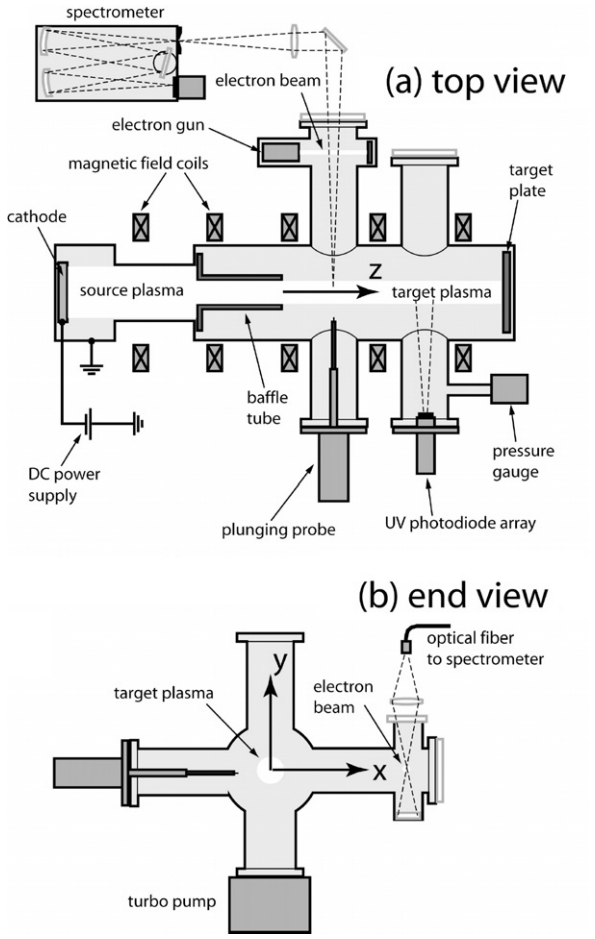

Fig. 1. (a) Top and (b) end views of PISCES-A linear divertor simulator experiment showing electron beam and spectrometer diagnostic.

measured with the spectrometer are shown in Fig. 2 for discharges with two different neutral pressures $P = 1$ and 18 mTorr. It can be seen that the plasma density profile falls off rapidly for radii $r \equiv |y| > 2$ cm or so. The plasma and neutral temperatures tend to be flatter across the plasma column. In principle, the plasma cooling rate due to neutral collisions can be obtained from analysis of the neutral temperature profiles; however, this is difficult with the data of Fig. 2 because the neutral radial cooling can hardly be resolved outside the scatter of the data.

To obtain a better signature of H_2 cooling, the H_2 temperatures in a side port are measured using the electron beam. The electron beam energy was 30–40 eV; this is far above the electron-impact excitation energy (≈15 eV) needed to excite the lines used. Small beam currents ($I_{beam} \approx 0.3$ mA) are

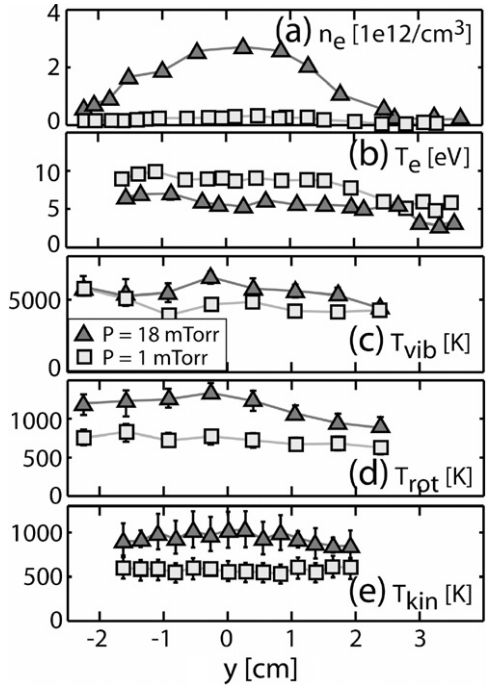

Fig. 2. Radial profiles of (a) electron density, (b) electron temperature, (c) H_2 vibrational temperature, (d) H_2 rotational temperature, and (e) H_2 kinetic temperature taken at target pressures $P = 1$ and 18 mTorr.

used to ensure that the electron beam does not significantly perturb the local H_2 temperatures. Compared with the plasma discharge current of about 40 A, the electron beam is expected to have a negligible effect.

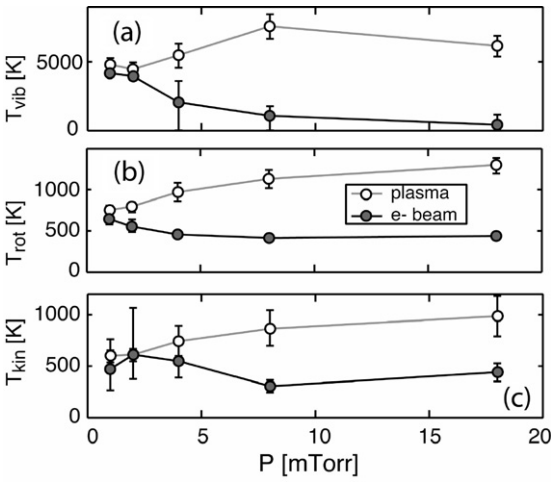

Fig. 3. H_2 temperature measurements in the plasma and in the side port as a function of neutral pressure P for (a) T_{vib}, (b) T_{rot}, and (c) T_{kin}.

Fig. 3 shows the H_2 temperatures (a) T_{vib}, (b) T_{rot}, and (c) T_{kin} measured in the plasma (open circles) and in the electron beam (filled circles) as a function of neutral pressure P. It can be seen that the temperatures in the main chamber and in the side port are quite close at low P, but diverge significantly as P is increased.

3. H_2 trajectory modeling

In order to interpret the measured H_2 vibrational, rotational, and kinetic temperatures obtained in spatial decay experiments, Monte-Carlo modeling of the H_2 trajectories in the PISCES-A vacuum chamber was performed. The model geometry included a section ($L = 12$ cm) of the main chamber tube, main (4) side ports, and a small side tube for the neutral pressure gauge at one axial location. Periodic boundary conditions were assumed at the axial ends of the model geometry section. Nonlinear Monte-Carlo modeling was used, i.e. the neutral density n_{H_2}, vibrational temperature T_{vib}, rotational temperature T_{rot}, and kinetic temperature T_{kin}, were updated periodically in response to time-averaged results during the simulation process. Neutral depletion by electron-impact dissociation and ionization of H_2 was included in the model. This was done by assigning the test particle an effective density, which was lowered at the expected density depletion rate due to dissociation and ionization as a function of time when the test particle passed through plasma elements. The resulting density loss term was compensated for by assuming an equal and opposite source of cold H_2 from the chamber walls (from recycling radial transport); this was implemented by increasing the particle effective density during wall collisions with the main chamber wall.

Cooling during wall collisions is treated as follows: at each H_2-surface collision, the neutral temperatures T_{vib}, T_{rot}, and T_{kin}, are assumed to have probabilities α_{VS}, α_{JS}, and α_{KS} of relaxing to the temperature of the cold stainless steel wall (assumed to be at room temperature $T_{wall} = 300$ K). The angular dependence of H_2-surface scattering is not known, so the scattering of direction of the velocity vector is assumed to be a mixture of 50% diffusive, 50% specular in wall collisions. The new direction vector for specular scattering $\hat{u}'_{spec}$ relative to the incident trajectory $\hat{u}$ is

$$\hat{u}'_{spec} = \hat{u} - 2\hat{n}_3(\hat{n}_3 \cdot \hat{u}), \quad (1)$$

where $\hat{n}_3$ is the local direction vector normal to the wall. The new direction vector for diffuse scattering is

$$\hat{u}'_{\rm diff} = \sqrt{\xi_1}\cos(2\pi\xi_2)\hat{n}_1 + \sqrt{\xi_1}\sin(2\pi\xi_2)\hat{n}_2 + \sqrt{1-\xi_1}\hat{n}_3, \quad (2)$$

where the ξ_i represent different random numbers, with $0 < \xi_i < 1$. If the sampling of the probability $\alpha_{\rm KS}$ indicates that the velocity magnitude is to be updated in a H_2-surface collisions, then the 2π Maxwellian velocity sampling is used

$$u' = u_{\rm wall}\sqrt{-\ln(\xi_1\xi_2)}, \quad (3)$$

where $u_{\rm wall} = \sqrt{2T_{\rm wall}/{\rm m}}$ is the most probable velocity for a Maxwellian at the wall temperature. Vibrational and rotational temperatures are treated statistically, i.e. the test particle is assigned temperatures $T_{\rm vib}$ and $T_{\rm rot}$, rather than actual quantum levels (V, J). The kinetic energy is treated individually, i.e. the kinetic temperature is calculated from the Maxwellian average of the velocity magnitude u through each element. Plasma heating of neutral temperatures is not calculated in the model; instead, measured values of $T_{\rm vib}$, $T_{\rm rot}$, and $T_{\rm kin}$ are enforced within the plasma volume. The plasma region itself is simulated as a top-hat profile, i.e. a constant electron density $\bar{n}_{\rm e}$ and electron temperature $\overline{T}_{\rm e}$ constant out to a radius $R_{\rm p} = 4$ cm is assumed. These values are chosen so that line-density and line-energy density of the measured profiles are conserved, i.e. $\int n_{\rm e} r{\rm d}r = \frac{1}{2}\bar{n}_{\rm e}R_{\rm p}^2$ and

$$\int n_{\rm e}T_{\rm e} r{\rm d}r = \frac{1}{2}\bar{n}_{\rm e}\overline{T}_{\rm e}R_{\rm p}^2.$$

The distance between each elastic scattering ($H_2 + H_2$) event is estimated as being $\lambda_i = \lambda_{\rm mfp}\ln\xi$, where $\lambda_{\rm mfp} = u/n_{\rm H_2}\langle\sigma u\rangle_{\rm elastic}$ is the $H_2 + H_2$ mean-free path evaluated at the test particle velocity u and the background temperature $T_{\rm kin}$. After an elastic scattering event, the velocity is re-sampled in 4π:

$$u' = u_0\sqrt{-\ln\xi_1}\times\left[2\sqrt{\xi_2(1-\xi_2)}\cos(2\pi\xi_3)\hat{x} + 2\sqrt{\xi_2(1-\xi_2)}\sin(2\pi\xi_3)\hat{y} + (1-2\xi_2)\hat{z}\right], \quad (4)$$

where $u_0 = \sqrt{2T_{\rm kin}/{\rm m}}$ is the most probable velocity for the local kinetic temperature.

The probability of rotational-kinetic energy exchange in each elastic collision is included using the calculations of Ref. [8]. Rotational–vibrational and vibrational-kinetic energy exchange rates in $H_2 + H_2$ collisions are thought to be small [9,10] and are ignored here.

Rotational–vibrational energy exchange during H_2-surface collisions is thought to be large, but only at larger kinetic energies ($T_{\rm kin} > 0.2$ eV [11] or $T_{\rm kin} > 1$ eV [12]) and is therefore ignored here. The neglect of vibrational–rotational coupling in the model is supported by the observed large ($\approx 5\times$) difference in $T_{\rm vib}$ and $T_{\rm rot}$ seen in Fig. 3. The atomic neutral H is expected to be found in small quantities here $n_{\rm H}/n_{\rm H_2} \approx 10^{-2}$ [13] and is therefore not included. Also, dissociation of H_2 in wall collisions is ignored, as this is thought to be negligible for kinetic energies $T_{\rm kin} < 1$ eV [12]. The simulations are run steady-state, where a single particle is followed until sufficient statistics are gathered in every element for modeling the spatial decay data. Fig. 4 shows the modeled H_2 temperatures obtained for two different target pressures $P = 1$ and 18 mTorr using accommodation probabilities $\alpha_{\rm VS} = 10^{-3}$, $\alpha_{\rm JS} = 10^{-3}$, and $\alpha_{\rm KS} = 10^{-2}$.

A qualitative estimate of the error resulting from the unknown angular distribution of H_2 leaving the surface is shown in Fig. 5. The simulated average number of neutral–neutral and neutral–surface collisions experienced by an H_2 neutral as it travels from the plasma ($x = 0$) to the electron beam location ($x = 62$ cm) is plotted as a function of target region neutral pressure P. Simulations run with purely diffuse surface collisions are plotted with solid curves, while simulations run with purely

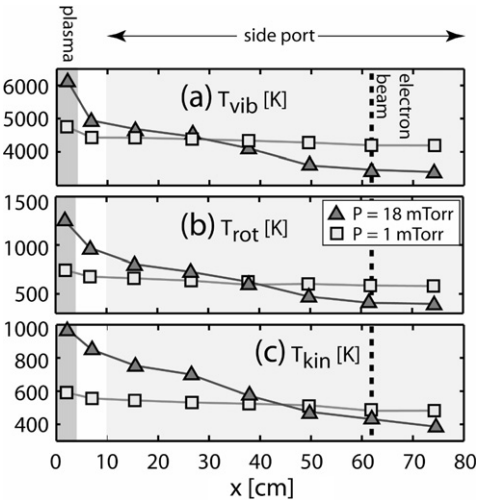

Fig. 4. Modeled (a) $T_{\rm vib}$, (b) $T_{\rm rot}$, and (c) $T_{\rm kin}$ as a function of radial position x moving from the plasma central axis down the side port for two neutral pressures P.

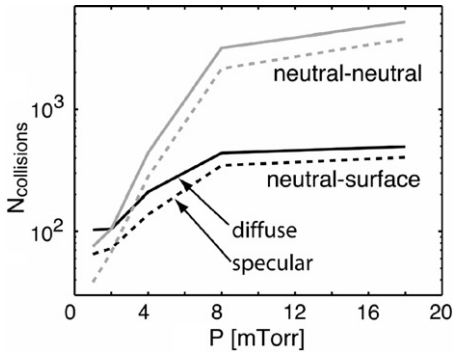

Fig. 5. Modeled average number of neutral–neutral and neutral–surface collisions experienced by a H_2 neutral as it travels from the plasma ($x = 0$) to the electron beam location ($x = 62$ cm).

specular surface collisions are plotted with dashed curves. It can be seen that the number of neutral–neutral collisions is larger for all but the lowest neutral pressures $P < 2$ mTorr. Accurate modeling of neutral–neutral collisions is therefore crucial for accurately capturing the neutral trajectories for $P > 2$ mTorr.

4. Comparison with experiment

The accommodation probabilities α_{VS}, α_{JS}, and α_{KS} are estimated by running the Monte-Carlo simulations to best match the measured temperatures T_{vib}, T_{rot}, and T_{kin} at the two points $r = 0$ and $r = 62$ cm with α_{VS}, α_{JS}, and α_{KS} varied as free parameters. Fig. 6 shows accommodation probabilities obtained assuming surface reflections are a mixture of 50% diffuse/50% specular. Error bars are estimated based on the scatter in the measured temperatures and on the uncertainty introduced in the modeling when using fully specular or fully diffuse wall reflections. It can be seen that the accommodation probabilities appear to increase at higher neutral pressures; the cause of this is not well-understood at present, but could result from wall heating or from an underestimate of the neutral–neutral scattering rate in the Monte-Carlo simulations. At $P = 18$ mTorr, the temperatures T_{rot} and T_{kin} become so strongly coupled that it is not possible to accurately separate α_{JS} and α_{KS} using the measured data, so it is assumed that $\alpha_{JS} = \alpha_{KS}$.

Once the accommodation rates are known, the steady-state power loss from the plasma due to neutrals can be estimated. For example, neutral vibrational heat flux to the walls is estimated as

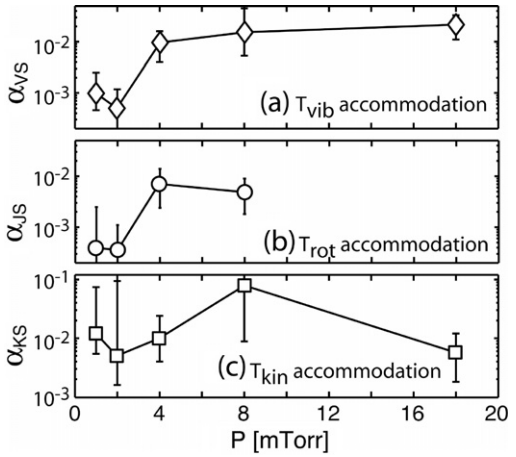

Fig. 6. Accommodation probabilities (a) α_{VS}, (b) α_{JS}, and (c) α_{KS} obtained from spatial decay experiments at different target region pressures.

$$q_{wall}(T_{vib}) \approx \frac{1}{4L} \int dS n_{H_2} v_{H_2} \alpha_{VW} T_{vib}, \quad (5)$$

where $v_{H_2} \equiv \sqrt{\frac{8T_{kin}}{\pi m_{H_2}}}$, $\int dS$ denotes a surface integral over the interior of the vacuum chamber, and L is the length of the vacuum chamber. Analogous equations are used for the rotational and kinetic heat flux.

Fig. 7 shows the resulting cooling rates per unit length to the plasma column due to neutral collisions. Also shown in Fig. 7 are the radiated power loss per unit length, measured with an AXUV photodiode array; and the radial heat loss due to plasma radial transport, measured with a fast-swept Langmuir probe; these measurements have been described in

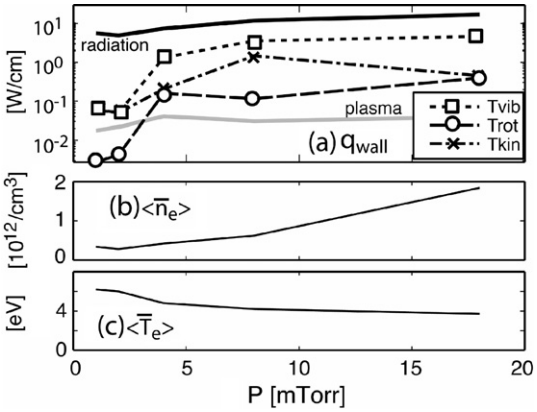

Fig. 7. (a) Radial flux to chamber wall, (b) profile and time-averaged electron density $\langle \bar{n}_e \rangle$, and (c) profile and time-averaged electron temperature $\langle \bar{T}_e \rangle$ as a function of neutral pressure P_{target}.

more detail previously [14]. It can be seen that the radiation cooling is the largest loss term, but neutral cooling becomes significant (within a factor two of radiation) at higher neutral pressures. Plasma heat flux to the walls is much smaller (≈100×) than radiation loss.

5. Discussion

This paper demonstrates that Monte-Carlo modeling, together with measurements of the spatial decay of the H_2 temperatures T_{vib}, T_{rot}, and T_{kin} down a side port, is a promising technique for estimating the accommodation probabilities in H_2-surface collisions. The resulting accommodation probabilities for T_{vib}, T_{rot}, and T_{kin} fall in the range $10^{-3} < \alpha_{VS} < 10^{-2}$, $10^{-3} < \alpha_{JS} < 10^{-2}$, $10^{-2} < \alpha_{KS} < 10^{-1}$. Overall, these values for α_{VS} and α_{JS} are qualitatively consistent with previous very indirect measurements using steady-state power balance in PISCES-A which found $\alpha_{VS} \approx \alpha_{JS} \approx 10^{-3}$ [15]. Accurate measurement of the accommodation coefficients are essential for hydrogen plasma edge modeling because corresponding theoretical estimates for these quantities can vary by orders of magnitude [16,17]. In the measurements presented here, the main sources of uncertainty are: scatter in the measured temperatures T_{vib}, T_{rot}, and T_{kin}; uncertainty in the diffuse vs. specular nature of the surface scattering; and the unexplained rise in the accommodation probabilities at higher neutral pressures. Future experiments will attempt to reduce these errors and apply this technique to different wall materials at different surface temperatures.

Acknowledgements

The technical support of L. Chousal, R. Hernandez, and T. Lynch is gratefully acknowledged. This work was supported by US DOE grants No. DE-FG03-95ER54301 and DE-FG03-00ER54568.

References

[1] T. Fujimoto, K. Sawada, K. Takahata, et al., Nucl. Fusion Lett. 29 (1989) 1519.
[2] A.Yu. Pigarov, Phys. Scripta T96 (2002) 16.
[3] S.I. Krasheninnikov, A.Yu. Pigarov, D.J. Sigmar, Phys. Lett. A 214 (1996) 285.
[4] W.M. Stacey, R.J. Groebner, Phys. Plasmas 13 (2006) 012513.
[5] D.M. Goebel, G. Campbell, R.W. Conn, J. Nucl. Mater. 121 (1984) 27.
[6] B.P. Lavrov, A.S. Melnikov, M. Kaening, J. Roepcke, Phys. Rev. E 59 (1999) 3526.
[7] Z. Qing, D.K. Otorbaev, G.J.H. Brussaard, et al., J. Appl. Phys. 80 (1996) 1312.
[8] D.R. Flower, E. Roueff, J. Phys. B: At. Mol. Opt. Phys. 31 (1998) 2935.
[9] V.A. Zenevich, G.D. Billing, J. Chem. Physics 111 (1999) 2401.
[10] M. Cacciatore, G.D. Billing, J. Phys. Chem. 96 (1992) 217.
[11] Z.S. Wang, G.R. Darling, S. Holloway, Surf. Sci. 458 (2000) 63.
[12] M. Cacciatore, M. Capitelli, G.D. Billing, Surf. Sci. 217 (1989) L391.
[13] E.M. Hollmann, A.Yu. Pigarov, Phys. Plasmas 9 (2002) 4330.
[14] E.M. Hollmann, A.Yu. Pigarov, Z. Yan, Phys. Plasmas 13 (2006) 052510.
[15] E.M. Hollmann, A.Yu. Pigarov, K. Taylor, J. Nucl. Mater. 337 (2005) 451.
[16] E.Ya. Kogan, V.N. Malnev, Sov. Phys. JETP 47 (1978) 276.
[17] A.M. Karo, J.R. Hiskes, R.J. Hardy, J. Vac. Sci. Technol. A 3 (1985) 1222.